

NEUTRON AND X-RAY SCATTERING FROM BIOLOGICALLY RELEVANT MATERIALS

by John Katsaras, Mu-Ping Nieh, Thad A. Harroun, Mukundan Chakrapani and Michael J. Watson

In the last few decades, or so, there has been a great deal of interest in the study of biologically relevant materials using various scattering techniques, in particular, neutron and x-ray diffraction. The use of these complementary techniques in conjunction with aligned biomimetic materials yields a wealth of structural information. The present contribution demonstrates the utility of these techniques to the general field of biophysics.

NEUTRON SOURCES

The existence of the neutral, subatomic, elementary particle called the neutron had been postulated since at least 1920, and it was discovered by James Chadwick in 1932. The neutron is found in all atomic nuclei except hydrogen (^1H), has a mass similar to

the proton, a nuclear spin of $\frac{1}{2}$, and a magnetic moment. Neutrons suitable for scattering experiments are presently being produced either by nuclear reactors (Fig. 1), where the fission of uranium nuclei results in neutrons of energies between 0.5 and 3 MeV, or by spallation sources (Fig. 2) where accelerated subatomic particles (e.g., protons) strike a target (e.g., tungsten or lead) releasing neutrons from the target material's nuclei.

The present contribution demonstrates the utility of various scattering techniques to the general field of biophysics.

In Canada, the 125 MW National Research Universal (NRU) reactor (Fig. 3) is located at Chalk River Laboratories, Ontario, and has a peak thermal flux of 3×10^{14} neutrons $\text{cm}^{-2} \text{sec}^{-1}$. NRU's fast MeV neutrons are produced from enriched fuel (*i.e.*, increased concentration of U-235 atoms), and are thermalized to an average energy of

~ 0.025 eV, using a "heavy" water moderator at room temperature. The neutron beams exiting the reactor are used to study a variety of condensed matter. The flux spectrum follows the Maxwell distribution, and can be shifted to higher energies, *i.e.* shorter wavelengths, by allowing the thermal neutrons to equilibrate with a "hot source" (e.g., the Institute Laue-Langevin [ILL], Grenoble, France, uses a self-heating graphite block at 2400 K), or shifted to lower energies with the use of a "cold source". The reactor at the National Institute of Standards and Technology (Gaithersburg, MD) produces cold neutrons by passing thermal neutrons through a vessel filled with liquid hydrogen at 40 K.

A more recent development is accelerator-based pulsed neutron sources whereby high energy subatomic particles, such as protons, are produced in a linear accelerator (Linac) and impinge on a heavy metal target releasing neutrons from the target material's nuclei. Since the Linac operation uses traveling electromagnetic waves, the arrival of the protons at the target are in pulsed bunches, and therefore the neutron beams produced are also pulsed. As with neutrons produced in a reactor, spallation neutrons have very high initial energies and must be slowed down from MeV to meV energies. However, their characteristic spectra differ considerably as the spallation source contains both a high energy "slowing" component and a thermalized component. Compared to reactor sources, the biggest advantage of spallation sources is that they produce much less heat per neutron. This low heat production/neutron translates into increased neutron fluxes. Nevertheless, since neutrons are produced in pulses, the time-averaged flux of even the most powerful pulsed source (e.g., ISIS, Oxford) is less than that of a high flux reactor source (e.g., ILL). However, judicious use of time-

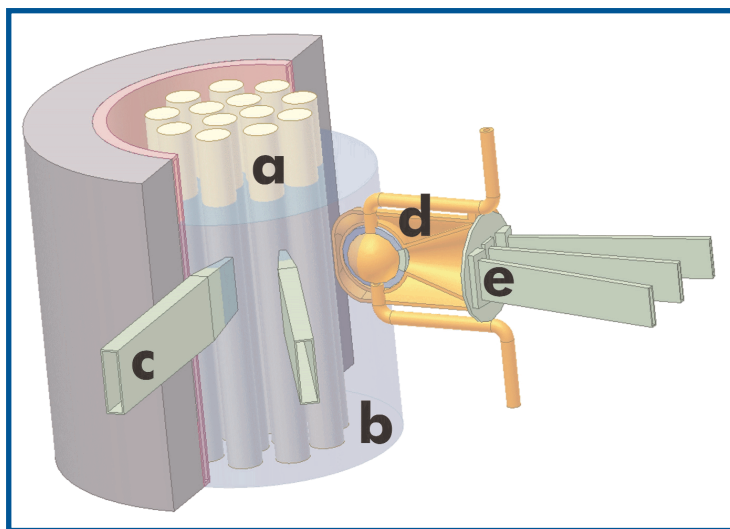


Fig. 1 Schematic of a nuclear reactor that produces thermal neutrons. Fuel rods (a) contain ^{235}U atoms which when they encounter moderated neutrons undergo fission producing ~ 2.5 high-energy neutrons/ ^{235}U atom. The probability of a fast (high energy) neutron interacting with a ^{235}U atom is small. To sustain the chain reaction, neutrons must be slowed down or "thermalized" by passing through a moderator. In practice, moderators such as H_2O , D_2O , graphite, or beryllium are used, filling the space in the reactor core around the fuel rods. For obvious reasons, H_2O is the most commonly used moderator (b). Thermal neutrons with a peak flux centered at ~ 1.2 Å can either be extracted directly from the reactor via a beam tube (c) or can be further slowed down by interaction with another, colder moderator, for example, a vessel of liquid hydrogen (d). These cold neutrons, with their Maxwellian distribution shifted towards lower energies, can be transported over many meters to the various spectrometers by ^{58}Ni coated optically flat glass surfaces (e) through a process known as total external reflection.

J. Katsaras (John.Katsaras@nrc-cnrc.gc.ca), M.-P. Nieh, T.A. Harroun, M. Chakrapani & M.J. Watson National Research Council, Steacie Institute for Molecular Sciences, Chalk River Laboratories, Chalk River, ON, K0J 1J0.



of-flight techniques, which can utilize the many neutron wavelengths in each pulse, can exploit the high brightness and can, for certain experiments, more than compensate for the time-averaged flux disadvantage. In the near future, the Spallation Neutron Source (SNS), presently being built at Oak Ridge National Laboratory (Oak Ridge, TN), will have a time-averaged flux comparable to the ILL reactor.

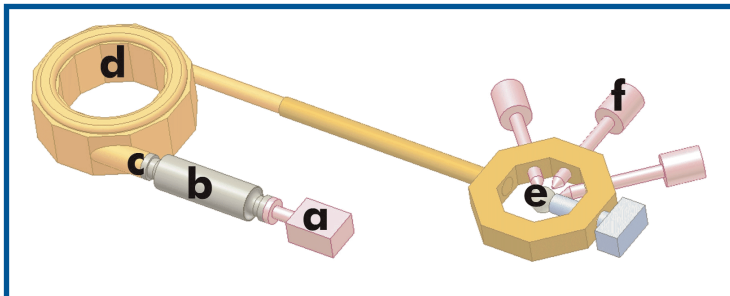


Fig. 2 Schematic of the Spallation Neutron Source (SNS) presently under construction at Oak Ridge National Laboratory, U.S.A. (a) H^+ ions produced by an ion source are accelerated to 2.5 MeV. (b) The H^+ ion beam is then delivered to a Linac further accelerating the 2.5 MeV H^+ ion beam to 1 GeV. (c) Prior to delivery from the Linac to the accumulator ring, H^+ ions are stripped of all of their electrons by a stripper foil resulting in H^{++} ions. (d) These H^{++} ions are bunched and intensified by the accumulator ring for delivery to the (e) liquid mercury target where a nuclear reaction takes place creating spallation neutrons for use at various spectrometers (f). The duration of the SNS proton pulse is 10^{-6} seconds and the repetition rate is 60 Hz. Not unlike reactor-based neutrons, spallation neutrons are moderated by either water or a liquid hydrogen source, giving rise to thermal or cold neutrons, respectively. The SNS chose mercury as the target for the proton pulses for the following reasons: 1) Unlike solid materials, liquid mercury does not experience radiation damage. 2) Mercury is a high atomic number material resulting in many spallation neutrons ($\sim 20 - 30$ neutrons/mercury atom). 3) Compared to a solid target, a liquid target at room temperature better dissipates heat and withstands shock effects.



Fig. 3 The National Research Universal (NRU) reactor located at Chalk River Laboratories and Canada's centrepiece for neutron scattering. The workers in the picture are standing above the reactor core cover plate, in front of the fuel rod extraction crane. NRU was Canada's 3rd nuclear reactor and went critical in 1957. It is a heavy water (D_2O) moderated and cooled reactor and is the major world source for medical isotopes (e.g., ^{99}Mo , ^{125}I , ^{131}I and ^{192}Ir). Originally, NRU had a power output of 200 MW. Presently, the reactor is rated at 125 MW and uses 20% enriched ^{235}U fuel.

X-RAY SOURCES

In 1895 Wilhelm Conrad Röntgen discovered x-rays by discharging electrical current in an evacuated glass tube generally known as a "Crookes tube". Over the next 60 years, the most common means of producing x-rays were by the impact of high-energy electrons, accelerated over several thousand volts in an evacuated glass tube, on to a metal anode. A tremendous improvement in x-ray production came with the development of the rotating anode. In this case the metal anode is fashioned as a rotating wheel, commonly made out of copper, that shows its circumference to the electron beam, thereby increasing the effective area bombarded by the electrons by factor of $2\pi r$ where r is the radius of the rotating wheel. The wheel is typically water-cooled internally, and since the heat is better dissipated, more electrons can impinge on the anode with a resultant tenfold increase in x-ray flux over a sealed tube with a fixed anode.

Synchrotron radiation is produced when a charged particle traveling at high speed undergoes acceleration, and was first observed in 1947 at General Electric's laboratories by Elder and co-workers^[1]. At first, this radiation was considered a nuisance

and wasted energy in particle physics research. However, in the 1960s it was recognized that this intense light could be used to carry out a variety of experiments. These machines today are commonly referred to as first-generation synchrotrons. First-generation sources operated in a so-called "parasitic" mode whereby condensed-matter physicists exploited the synchrotron light while high-energy physicists used the electron beam for their experiments.

In the 1970s and 1980s synchrotrons were constructed solely for their ability to generate synchrotron radiation. These so-called second-generation synchrotrons were large circular rings where charged particles such as, electrons or positrons were guided around the ring through a series of bending magnets at nearly the speed of light. As the magnets alter the electron's path, the electrons are accelerated towards the centre of the ring, and therefore emit synchrotron radiation. Examples of second-generation synchrotron sources are Brookhaven's National Synchrotron Light Source (NSLS, Upton, NY), commissioned in 1984, and The Photon Factory (Tsukuba, Japan).

The latest, third-generation synchrotrons (Fig. 4) such as the Advanced Photon Source (APS, Chicago, IL) and the European Synchrotron Radiation Facility (ESRF, Grenoble, France) are

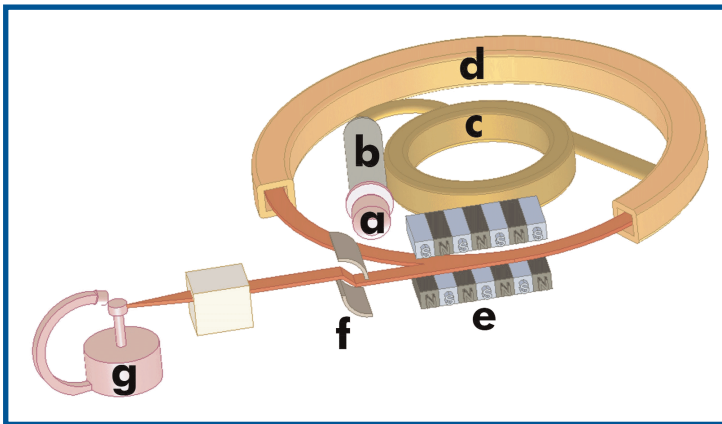


Fig. 4 Schematic of a third generation synchrotron source and its components: (a) An electron gun produces electrons which are catapulted by a (b) linear accelerator (Linac) from a standing start to nearly the speed of light ($\sim 300,000$ kms). (c) The booster synchrotron, as its name implies, "boost" the electrons from the Linac, to 99.999994 % of the speed of light. (d) Electrons are transported to the storage ring where they circulate for hours in a very high vacuum environment. Bending magnets direct the electrons around the ring. (e) Wigglers and undulators, commonly known as insertion devices, are placed in the straight sections of the storage ring and produce the brightest synchrotron light. (f) Beamlines "steer" the x-rays to the experiment through a series of mirrors. (g) The experimental station is where the x-rays strike the sample and are detected.

10^{10} times brighter (photons/ s / mm^2 / mrad^2) than first-generation synchrotron sources and 10^{15} times brighter than conventional sealed tubes and rotating anodes (Fig. 5). This increased brightness has been achieved through the use of insertion devices known as wigglers and undulators. Wigglers consist of a series of high field magnets placed above and below the electron beam along a straight section of the storage ring (Fig. 5). The magnets cause the electrons to undulate with a tighter radius, increasing the light emitted by the electrons at shorter wavelengths. Undulators are similar to multipole wigglers, but with a larger number of poles. The effect is that strong interference occurs between the radiation from consecutive magnets, which results in a spectral profile with a peak at a specific wavelength. The energy of the emitted x-rays can be tuned by changing the gap between the magnet poles.

The first synchrotron source in Canada, aptly named the Canadian Light Source (CLS), is a 2.9 GeV third-generation synchrotron source, which is presently being constructed in Saskatoon, at the University of Saskatchewan. It will be fully competitive with the best international sources and is expected to attract industrial and academic researchers. The CLS is scheduled for completion in 2004 at a cost of \$175 million. For further details about the science that will be carried out please refer to the article by Mike Jackson.

COMPARING NEUTRON AND X-RAY SCATTERING

X-ray radiation is an electro-magnetic wave, and so interacts most strongly with charged particles. Since the proton is 1000 times more massive than the electron, for an atom in most condensed materials, it is the electrons that interact most strongly with x-rays. The atomic form factor is a measure of the scattering strength of an element, and scales with Z , the number of electrons in the element, which is also the atomic number.

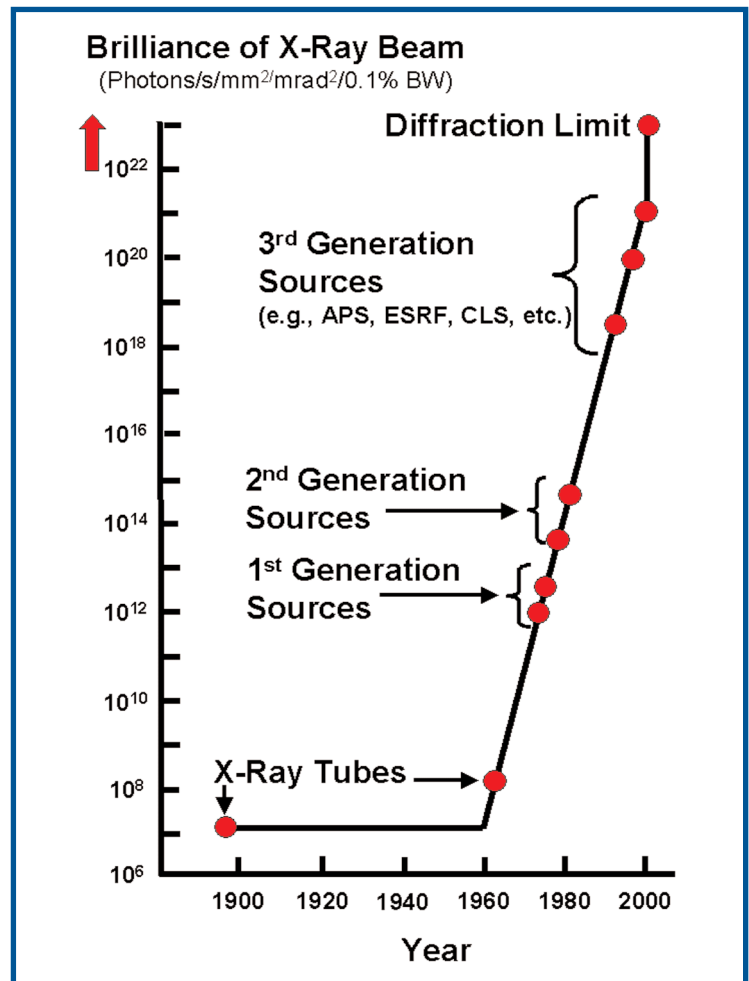


Fig. 5 Brilliance (photons/s/mm²/mrad²/0.1% band width) of x-ray beams as a function of time. As can be seen, present synchrotron technology is fast approaching its diffraction limit. The diffraction limit spot size is proportional to the wavelength and the focal length divided by the beam width. The next class of machines conceived to create intense x-rays beam are the so-called Free Electron Lasers (FELs). FELs will be capable of producing pulses ($60 - 360 \text{ s}^{-1}$) of coherent x-ray photons with fluxes orders of magnitude ($10^{11} - 10^{12}$) more intense when compared to the present 3rd generations synchrotron sources.

Neutrons on the other hand, are neutral, and therefore when they interact with other particles and atoms, must do so through direct contact. This means that the neutron is more likely to encounter the massive, fixed nuclei of atoms than an electron in the electron cloud. The interaction between the neutron and atomic nuclei involve the interactions between the nuclear spins and magnetic moments. For this reason, there is no relation between the atomic number and its ability to scatter neutrons. Neutron scattering ability is randomly distributed throughout the periodic table (*e.g.*, neutrons scatter equally well from N, Cl, Fe and Pt). Also, different isotopes of the same element may have radically different abilities to scatter neutrons.

Atomic nuclei are characterized both by an incoherent and a coherent neutron scattering length. The coherent scattering length is analogous to the atomic form factor in x-rays, while there is no x-ray analogue for the incoherent scattering length.

For the purposes of this review, we will only consider the case where the nuclear moments of the material being probed with neutrons are completely disordered, giving rise to so-called coherent scattering.

Compared to x-rays, the biggest disadvantage of neutrons is that neutron fluxes from reactor or even spallation-based sources are minuscule compared to x-ray fluxes produced at synchrotron facilities. This means experiments can take much longer to achieve the same signal-to-noise values. Moreover, the availability of neutron sources is scant compared to the combined availability of portable x-ray sources (e.g., sealed tubes and rotating anodes) and synchrotrons. Nevertheless, neutrons can "see" light atoms (e.g., H) equally well as "heavy" elements, whereas x-rays scattering is dominated by the heavier elements with many electrons in the sample. Further, neutrons can exploit isotopic substitution, such as deuterium for hydrogen, making neutrons an attractive probe for a variety of hydrogenous materials.

ELASTIC SCATTERING

For the purposes of this review we will limit ourselves to elastic scattering where the incident neutron or x-ray energy is equal to the energy after it has been diffracted. The wave vector \mathbf{k} , points in the direction of the beam, and has magnitude $|\mathbf{k}| = 2\pi/\lambda$, where λ is the wavelength of the neutrons or x-rays. The scattering vector \mathbf{Q} , is the difference between the incident and final wave vectors, $\mathbf{k}_i - \mathbf{k}_f$, and is schematically represented for a crystalline material in Fig. 6. From the Figure, one can easily derive Bragg's law for equally spaced planes of atoms separated by a distance d . To observe a diffraction peak, the Laue condition, $\mathbf{Q} = \mathbf{G}$, where \mathbf{G} is a reciprocal-lattice vector, must be met. Analytically, one can derive Bragg's Law from the magnitude of the scattering vector $|\mathbf{Q}|$. From Fig. 6 we observe that $|\mathbf{Q}| = 2k \sin\theta$ where 2θ is the angle between the incident beam and diffracted beam. Since $k = 2\pi/\lambda$ and the magnitude

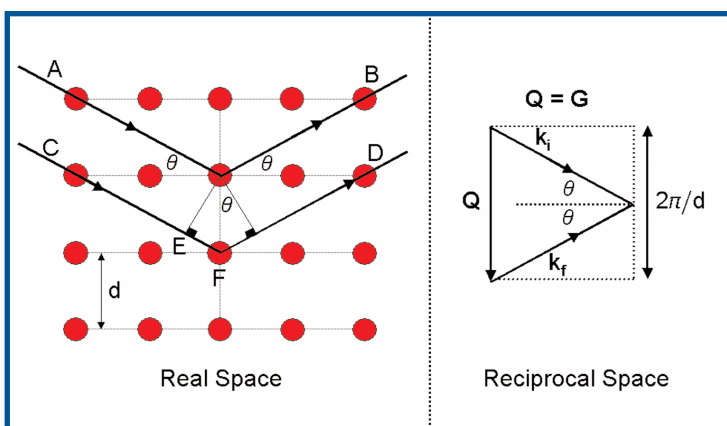


Fig. 6 The equivalence of Bragg' Law (real space) and the Laue condition (reciprocal space) for a two-dimensional square lattice. In the Bragg condition, neutrons or x-rays are specularly reflected from planes of atoms separated by a distance, d . The requirement for constructive interference between two waves emanating from different planes is that the path length difference is an integer number of the wavelength (λ) leading to the well-known expression $\lambda = 2d\sin\theta$. The Laue condition requires that $\mathbf{Q} = \mathbf{G}$ (constructive interference). Since $|\mathbf{G}| = 2\pi/d$, $|\mathbf{Q}| = 2k \sin\theta$ and $k = 2\pi/\lambda$, it then follows that $\lambda = 2d \sin\theta$, commonly known as Bragg's law (please see section on Elastic Scattering for further details).

of the reciprocal-lattice vector $|\mathbf{G}| = 2\pi/d$, carrying out the appropriate substitutions to $|\mathbf{Q}| = 2k \sin\theta$ results in $\lambda = 2d \sin\theta$, commonly known as Bragg's law. Simply, this is the condition for constructive interference of waves with incident angle θ on a set of equidistant planes separated by a distance d .

From the Bragg's law, it is possible to derive the concept of the structure factor for a crystal. The structure factor represents the cumulative scattering of the electrons or nuclei in a real sample and the effects of their arrangement within the sample. Such a derivation is beyond the scope of this review, however the result is straightforward; The structure factor \mathbf{F} , is the Fourier transform of the arrangement of the atoms in the sample, $\rho(x,y,z)$. The function \mathbf{F} is in general a complex function, with both real and imaginary parts. The imaginary part is related to the "phase" of \mathbf{F} . However, the intensity of the detected scattered radiation, \mathbf{I} , is proportional to the magnitude of \mathbf{F} , $\mathbf{I} = |\mathbf{F}|^2$, meaning the phase of \mathbf{F} is not detected. This is described as the "phase problem" in crystallography. Through various techniques, one can determine the phases of \mathbf{F} , and inverse Fourier transform to reconstruct the arrangement of atoms in the sample.

BIOMATERIALS

A biomaterial can be any substance, synthetic or natural in origin, found within or suitable for use in a biological system. For the present article, we focus on the biomaterials found in cell membranes, principally lipid assemblies. Lipids (Fig. 7) are biologically relevant amphipathic molecules - having a hydrophilic headgroup and hydrophobic hydrocarbon tails - and constitute $\sim 50\%$ of the mass of animal cellular membranes^[2], while the remaining mass is accounted for by proteins. The most common lipids have a polar headgroup and two fatty acid chains that can differ in length and degree of unsaturation (presence or absence of double bonds). Normally, the shorter of the two tails is saturated (no double bonds) while the longer hydrocarbon chain contains one or more double bonds. Difference in the length, saturation of the hydrocarbon chains and chemical make up of the headgroups all conspire to influence the packing of the lipid molecules, resulting in a variety of structural phases^[3,4].

NEUTRON SCATTERING IN THE PRESENCE OF A MAGNETIC FIELD

Compared to liposomal, or non-aligned, preparations, aligned stacks of lipid bilayers have allowed us to gain new insights into the structure of a variety of lipid phases^[5-7]. In the last few years there has been a great deal of interest in bilayers composed of short-chain (e.g., dihexanoyl phosphatidylcholine, DHPC) and long-chain lipids (e.g., dimyristoyl phosphatidylcholine, DMPC) that can be aligned in the presence of an applied magnetic field^[8-10]. It was observed that such lipid mixtures formed disc shaped bilayered micelles, and so-named bicelles. The short-chain DHPC lipid stabilizes the edge of the bicelle while the long-chain DMPC lipid populated the two major surfaces. In the presence of a magnetic field, these bicelles would orient with their bilayer normal perpendicular to the external magnetic field. Compared to lipid bilayers aligned on a solid support, the bilayered micelles were easily prepared and hydrated under physiologically relevant conditions, generally understood as being the following: a) The lipids, which form the bilayer, are in the disordered liquid - crystalline, $L\alpha$ phase undergoing rapid translational diffusion

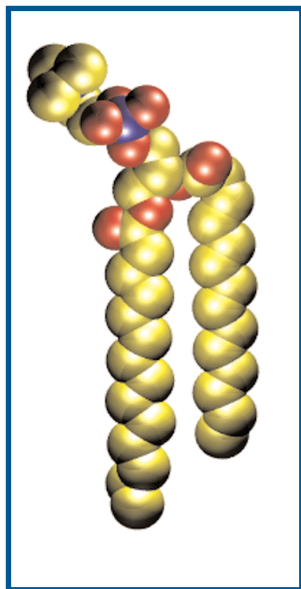


Fig. 7 Chemical model of the phospholipid dimyristoyl-phosphatidylcholine (DMPC). This lipid is composed of a hydrophilic phosphorylcholine headgroup, a glycerol backbone, and two hydrophobic saturated hydrocarbon chains. DMPC is comprised of carbon (yellow), oxygen (red), phosphorous (blue), nitrogen (hidden) and hydrogen atoms (not shown).

and *trans-gauche* isomerizations of their fatty acyl chains. b) The aqueous environment reflects relevant physiological ionic strength and pH. Nevertheless, these samples formed a cylindrical "powder" about the magnetic field.

In 1996, Prosser *et al.* [11-13] discovered that by doping the bilayered micelles with paramagnetic ions such as, Tm^{3+} , Eu^{3+} , etc., the bicelles "flipped" such that their bilayer normal were now parallel to the applied magnetic field, resulting in sharp single nuclear magnetic resonance (NMR) line. However, the question that remained unanswered from the NMR experiments was whether the resultant phase was a nematic (phase where the lipid aggregates have no positional order but tend to point in the same direction) or a smectic phase (aggregates have both positional and orientational order), a question that could unambiguously be answered by neutron scattering.

Neutron scattering experiments were carried out at the NRU reactor (Fig. 3) using the C5 and N5 (Fig. 8) triple-axis spectrometers and thermal neutrons of wavelength 2.37 Å from the (002) reflection of a pyrolytic-graphite monochromator [14]. The sample was aligned using a 2.6 T horizontal field superconducting magnet/cryostat. Figure 9a shows the diffraction pattern of a DMPC/DHPC lipid mixture doped with Tm^{3+} paramagnetic ions in the absence of an applied

magnetic field. The scattering curve contains a couple of quasi Bragg reflections, the first one centered at $Q \sim 0.05 \text{ \AA}^{-1}$. The positions of the peaks show the presence of a repeat unit of dimension $Q = 2\pi/d$ or $d \sim 126 \text{ \AA}$, while the width of the scattering peak is indicative of how many such structural units are contributing coherently, and is a measure of the correlation length of the sample. The inset to Fig. 9a depicts a rocking curve with a FWHM of $\sim 90^\circ$, indicative of poorly aligned lipid multibilayer stacks. However, upon applying a 2.6T field the scattering curve goes from being somewhat featureless to exhibiting a number of well-defined quasi Bragg peaks (5 in total).

The position of the first quasi Bragg peak is again centred at $Q \sim 0.05 \text{ \AA}^{-1}$, similar to the same sample in the absence of an applied field, while the other peaks occur at $2Q$, $3Q$, etc. Moreover, the inset to Fig. 9b depicts a rocking curve with a FWHM of $< 1.0^\circ$, proof that the system is now highly aligned. The magnetic field, in this case, acts to align the lipid multibilayer stacks. On the other hand, removal of the Tm^{3+} ions results in a phase transition from a smectic to a nematic phase [14], as shown in Fig. 9c.



Fig. 8 The N5 triple-axis spectrometer located at the NRU reactor, Chalk River Laboratories (CRL), shown in triple-axis mode with the 2.6 Tesla M2 vertical field superconducting magnet/cryostat sitting atop a rotating table. The triple-axis spectrometer, invented in 1950s in Canada by Bertram N. Brockhouse, consists of three independently controlled axes of rotation for the sample, monochromator, and analyzer crystals.

From the studies carried out at Chalk River using thermal neutrons and small-angle neutron scattering (SANS) studies performed at the National Institute of Standards and Technology (NIST) with cold neutrons [15,16], we have arrived at the following scenario: At temperatures below $\sim 310 \text{ K}$ the system forms an isotropic micellar solution for all of the lipid concentrations studied. However, at temperatures $> 310 \text{ K}$ the system forms either monodispersed unilamellar vesicles at low lipid concentrations ($C_{lp} < 0.025 \text{ g/ml}$) while a lamellar phase perforated with holes is formed at lipid concentrations $> 0.025 \text{ g/ml}$. The various phases are shown schematically in Fig. 10. Since then we have carried out a number of neutron studies further revealing the rich phase behaviour of lipid mixtures containing short and long chain PC lipids [17-19].

THE INFAMOUS "VAPOUR PRESSURE PARADOX" ELUCIDATED USING NEUTRON SCATTERING

Compared to "powder" or non-aligned samples, aligned preparations allow us to differentiate between in-plane (*e.g.*, hydrocarbon chain organization) and out-of-plane (*e.g.*, lamellar repeat spacings) structure. Aligned samples also accelerated data collection in the absence of a two-dimensional detector, and reduce the need for larger samples. This is especially important when certain sample preparations are available only in small quantities such as deuterated compounds, and expensive peptides and proteins. Nevertheless, despite the many advantages offered by aligned samples their use has not been widely reported.

A common method of preparing aligned lipid bilayers is to deposit them on to a solid substrate (*e.g.*, single crystal of silicon, mica or glass) from a concentrated lipid/solvent solution, and allowing the solvent to evaporate [20,21]. Typically, such samples are then hydrated by exposure to water vapour. Such samples, however, fail to take up as much water between the bilayers as samples prepared in water [22]. This difference between the two sample preparations could not be explained, as the chemical activity of water vapour, at 100% relative

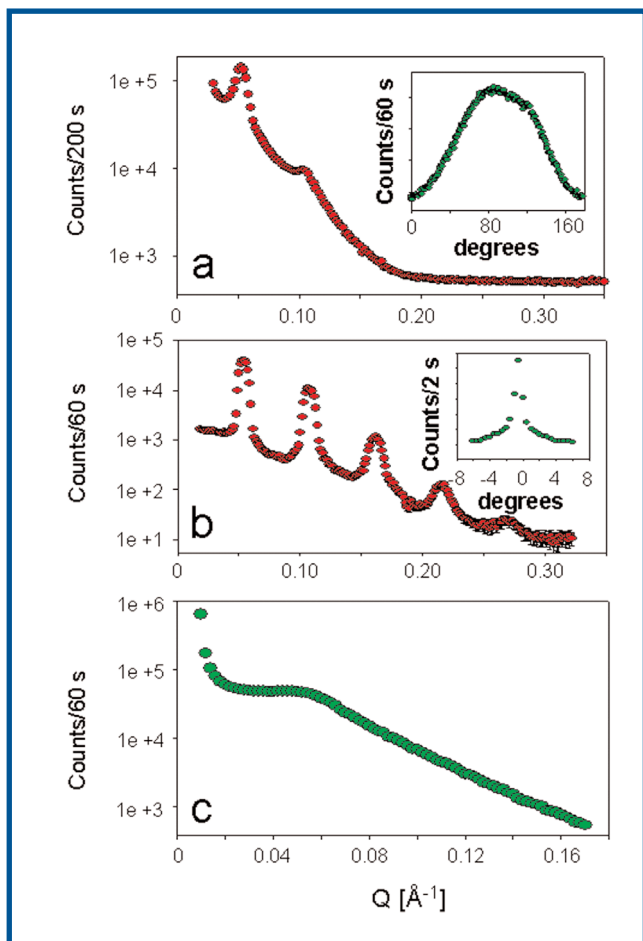


Fig. 9 (a) Diffraction pattern of DMPC/DHPC bilayers doped with the paramagnetic lanthanide ion, Tm^{3+} in the absence of a magnetic field and at a temperature, T , of 315 ± 1 K. The inset to (a) depicts the rocking curve and is a direct measure of the alignment of the lipid bilayers. (b) Diffraction pattern on application of a 2.6 T magnetic field to the system in (a). The rocking curve (inset) indicates that the system is much better aligned in the presence of a magnetic field. $T = 315 \pm 1$ K. (c) The non-doped DMPC/DHPC system in the presence of a magnetic field. It is clear that doping the system with Tm^{3+} induces a nematic-smectic transition, while the magnetic field aligns the system. For further details please see reference [14].

humidity (RH), is the same as that of bulk water. Consequently, this discrepancy became widely known as the "vapour pressure paradox" (VPP). Since it is generally believed that biological systems are under conditions of "excess water" (which may not always be true), the fact that the aligned systems could not be fully hydrated may have been one reason for their limited use in biophysical studies.

Without exception, the vapour pressure paradox has persisted over the last three decades [23], and was in recent years justified on theoretical grounds [22]. However, the solution to the paradox was provided using neutron scattering and a suitable aluminum sample cell designed to minimize temperature gradients (Fig. 11a). It was found that samples aligned on a substrate and hydrated from water vapour exhibited repeat spacings no different than those of samples immersed in water [23].

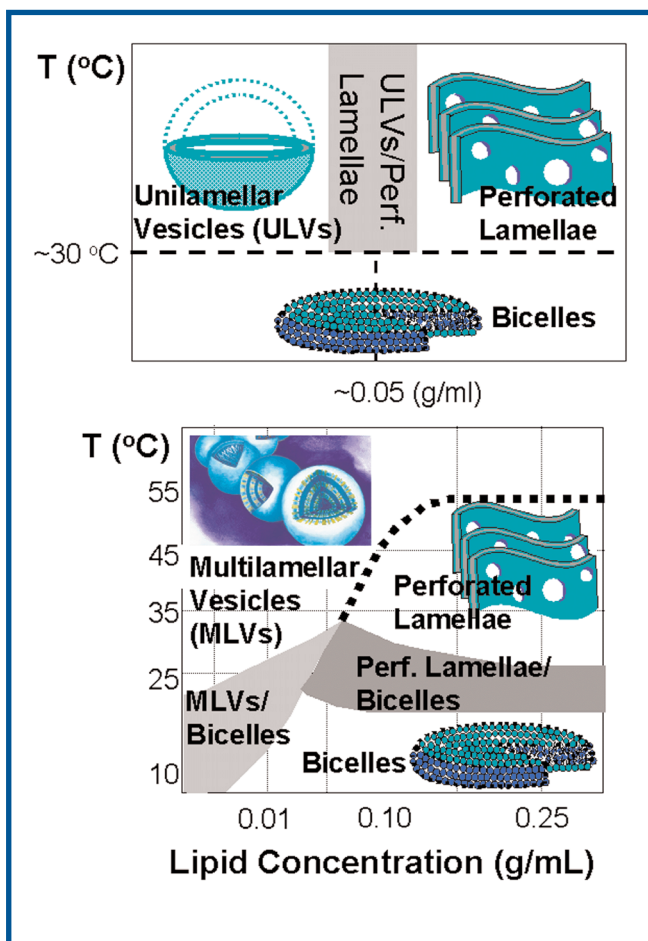


Fig. 10 Phase diagrams of the Tm^{3+} doped DMPC/DHPC system (top) and the non-doped DMPC/DHPC system as determined by small-angle neutron scattering (SANS). The experiments, for the most part, were performed using cold neutrons ($\lambda = 6 - 8$ Å) on the 30 m SANS at the National Institute of Standards and Technology (NIST) in Gaithersburg, MD. For further details please see references [15] and [16].

was an artifact of poorly designed sample environments.

THE MYSTERY OF THE SYMMETRIC RIPPLE AND SYNCHROTRON RADIATION

The solution of the vapour pressure paradox and the experience gained from it allowed us to extend the neutron sample cell design to one suitable for x-ray diffraction. One outstanding issue that could be resolved using fully hydrated aligned samples was whether or not bilayers of dipalmitoyl phosphatidylcholine (DPPC) formed, upon cooling, a mixture of short and long wavelength rippled bilayers or simply a single population long wavelength rippled bilayers [26]. Moreover, there were discrepancies in the literature with regards to the lattice parameters describing the possible ripple phases [27-29].

Certain class of well-hydrated lipid bilayers, such as phosphatidylcholines, often exhibit a thermodynamic phase commonly known as the ripple or P_{β} phase. This phase occurs between the lower temperature L_{β} phase and the higher temperature disordered L_{α} phase. It is generally agreed upon that on increasing temperature, L_{β} bilayers form asymmetric rip-

Moreover, it was also shown later that a vestigial VPP could also not explain the historical experimental results [24]. It was therefore shown, that the deficiencies in previous sample cell designs (e.g., presence of large thermal gradients) allowed for relative humidities of no greater than 99% [25], giving rise to the infamous vapour pressure paradox. The fact that neutrons interact differentially with various nuclei allowed us to design a sample environment that conclusively demonstrated that the vapour pressure paradox

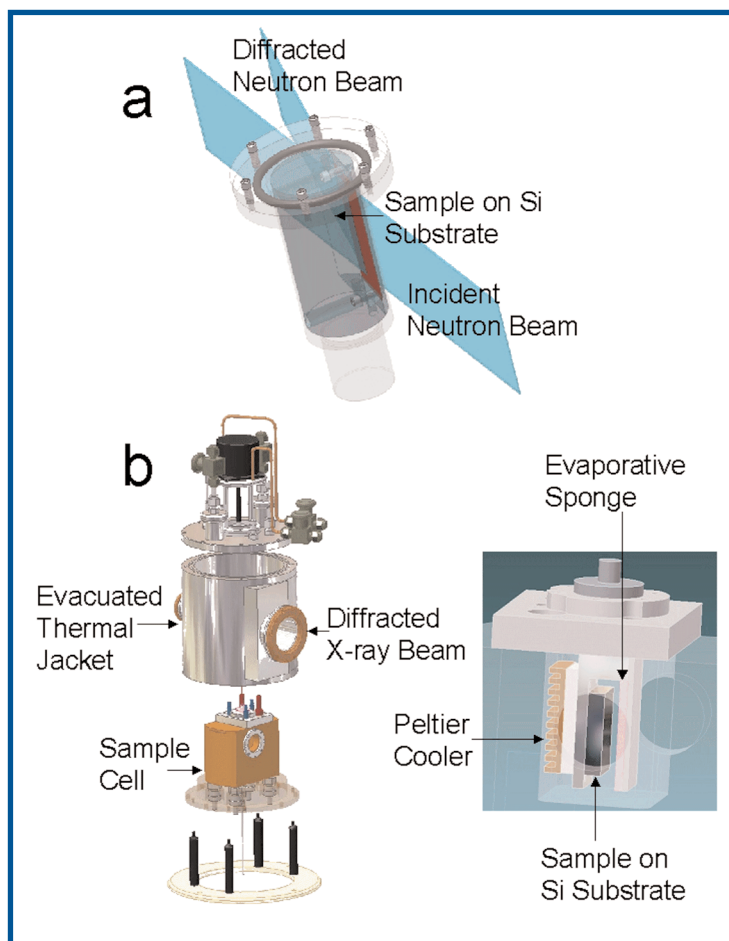


Fig. 11 (a) Neutron sample cell capable of achieving 100% relative humidity, and thus fully hydrating aligned lipid multibilayers from water vapour. (b) The equivalent of the sample cell in (a) but suitable for x-ray diffraction. The complexity of the x-ray cell is evident, and this is due to the fact that x-rays are generally, not as "penetrating" as neutrons. For further details please see references [23] and [31].

ples whose profile is somewhat akin to a sawtooth function, rather than a simple sinusoidal shape, and exhibit a wavelength of $\sim 140 \text{ \AA}$ [26-29]. However, upon cooling from the high temperature L_α phase, the P_β phase of DPPC bilayers contains a mixture of long wavelength rippled bilayers coexisting with the usual short wavelength rippled bilayers [26-28]. This scenario was put in question by the re-analysis of previously published x-ray powder diffraction data and newly acquired neutron powder diffraction data. The authors concluded that both x-ray and neutron powder diffraction data were consistent with a single long wavelength ripple phase [30].

In order to resolve this issue, a new sample environment was developed at Chalk River suitable for x-ray diffraction and capable of fully hydrating lipid bilayers [Fig. 11b] so that their bilayer repeat spacings were indistinguishable from those bilayers immersed in water [31]. Using aligned samples the resultant diffraction patterns could be clearly indexed in reciprocal space without any of the ambiguities associated with powder diffraction data. The experiments were carried out at the Cornell High Energy Synchrotron Source (CHESS, Ithaca, NY) using monochromatic x-rays ($\lambda = 1.38 \text{ \AA}$) and 2D charge coupled device (CCD) detector. The flux at the sample was determined to be $\sim 10^{12} \text{ photons mm}^{-2} \text{ s}^{-1}$ and exposures varied

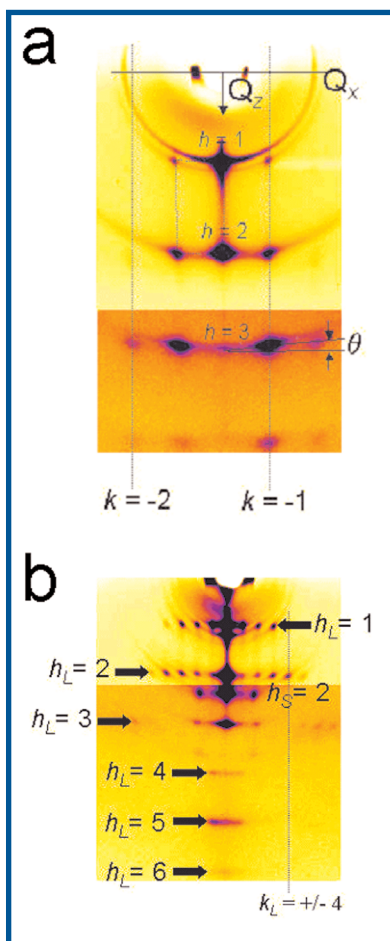


Fig. 12 Two-dimensional diffraction patterns at 312 K of asymmetrically (saw-tooth) rippled bilayers (a) and a mixture of asymmetrical and symmetrical lipid bilayers (b). Q_z is normal to the lipid bilayers while Q_x is in the plane of the bilayers. The lamellar reflections are denoted by h (the subscripts L and S stand for long and short wavelength ripples, respectively) while the off specular ripple reflections are denoted by k . The angle made by the off specular ripple reflections with the Q_z axis, is denoted by θ . $\theta \neq 0^\circ$ is indicative of asymmetric ripples (a) while $\theta = 0^\circ$ is indicative of symmetric ripples (b). The data were collected at the Cornell High Energy Synchrotron Source (CHESS, Ithaca, NY) using 1.38 \AA photons and the sample cell shown in Fig. 11(b). For further details please see reference [26].

from 0.1 to 15 s [26].

From the 2D diffraction patterns [Fig. 12] it is clear that upon heating both chiral and racemic DPPC bilayers form one population of rippled bilayers, as all reflections can be indexed to one unique unit cell. However, upon cooling the situation is very different. The data in Fig. 12 supports the commonly accepted notion by Yao *et al.* [27] and Matuoka *et al.* [28] that there are two distinct, coexisting populations of ripples differing in d , ripple wavelength, and ripple symmetry. Moreover, direct evidence for the existence of the symmetric ripple was provided, for the first time, using synchrotron radiation [26].

CONCLUDING REMARKS

Canada has an outstanding tradition in neutron scattering that began prior to the Nobel prize winning research of B.N. Brockhouse. The NRU reactor, located at Chalk River Laboratories, is the primary source of thermal neutrons suitable for most condensed matter experiments. The National Research Council's (NRC's) Neutron Program for Materials Research operates Canada's Neutron Beam Laboratory, a resource for universities, industry, and government laboratories. Access to the laboratory is granted free of charge to users whose research is destined for the public domain. For proprietary research, access is arranged through a fee-for-service agreement.

Presently, there are efforts to replace NRU with a neutron source capable of producing cold neutrons that are better suitable for studying large molecules commonly found in biology.

Unit now, Canada has been the only G8 country without a synchrotron source. This will no longer be the case

once the 2.9 GeV CLS is turned on in 2004. The CLS will be one of only a handful of third-generation synchrotrons in the world. The initial suite of instruments located at the CLS will include the following: a) Three infrared beamlines with photon energies of between 0.006 eV and 3 eV. b) High resolution Spherical Grating Monochromator beamline (100 eV - 2000 eV), presently located at Madison, Wisconsin. c) Soft X-ray Spectromicroscopy beamline (100 eV - 2000 eV). d) Protein Crystallography beamline (3 keV - 40 keV). e) Hard x-ray, general purpose XAFS (X-ray Absorption Fluorescence Spectroscopy) beamline (3 keV - 40 keV). The CLS will be Canada's national facility for synchrotron and will serve the Canadian user community in a similar fashion as NRU is doing presently for neutrons.

In this article we have discussed how neutrons and x-rays are produced and the properties that make them unique probes. We hope to have imparted to the reader the notion that neutrons and x-rays are complimentary probes and have shown, through various examples, some problems that can be effectively tackled through the use of neutron and x-ray scattering techniques.

REFERENCES

1. F.R. Elder, A.M. Gurewitsch, R.V. Langmuir, and H.C. Pollock, "Radiation from Electrons in a Synchrotron", *Phys. Rev.* **71**:829-830 (1947).
2. L. Stryer, "Biochemistry", W.H. Freeman and Company, San Francisco (1981).
3. P. Yeagle (ed), "The Structure of Biological Membranes", CRC Press, Boca Raton, FL (1992).
4. J. Katsaras and T. Gutberlet (eds), "Lipid Bilayers: Structure and Interactions", *Biological Physics Series*, Springer, Germany (2001).
5. V.A. Raghunathan and J. Katsaras, "Structure of the L_c Phase in a Hydrated Lipid Multilamellar System", *Phys. Rev. Lett.* **74**:4456-4459 (1995).
6. J. Katsaras and V.A. Raghunathan, "Molecular Chirality and the "Ripple" Phase of Phosphatidylcholine Multibilayers", *Phys. Rev. Lett.* **74**:2022-2025 (1995).
7. J. Katsaras, "Structure of the Subgel (L_c) and Gel (L_β) Phases of Oriented Dipalmitoylphosphatidylcholine Multibilayers", *J. Phys. Chem.* **99**:4141-4147 (1995).
8. C.R. Sanders II and J.P. Schwonek, "Characterization of Magnetically Orientable Bilayers in Mixtures of Dihexanoylphosphatidylcholine and Dimyristoylphosphatidylcholine by Solid State NMR", *Biochemistry*, **31**:8898-8905 (1992).
9. C.R. Sanders II, B.J. Hare, K.P. Howard, and J.H. Prestegard, "Magnetically-Oriented Phospholipid of Micelles as a Tool for the Study of Membrane-Associated Molecules", *Prog. NMR Spectro.*, **26**:421-444 (1994).
10. C.R. Sanders II and J.H. Prestegard, "Magnetically Orientable Phospholipid Bilayers Containing Small Amounts of a Bile Salt Analogue, CHAPSO", *Biophys. J.*, **58**:447-460 (1990).
11. R.S. Prosser, S.A. Hunt, J.A. DiNatale, and R.R. Vold, "Magnetically Aligned Membrane Model Systems with Positive Order Parameter: Switching the Sign of S_{zz} with Paramagnetic Ions." *J. Am. Chem. Soc.*, **118**:269-270 (1996).
12. R.S. Prosser, J.S. Hwang, and R.R. Vold, "Magnetically Aligned Phospholipid Bilayers with Positive Ordering: A New Model Membrane System", *Biophys. J.*, **74**:2405-2418 (1998).
13. R.S. Prosser, V.B. Volkov, and I.V. Shiyonovskaya, "Novel Chelate- Induced Magnetic Alignment of Biological Membranes", *Biophys. J.*, **75**:2163-2169 (1998).
14. J. Katsaras, R.L. Donaberger, I.P. Swainson, D.C. Tennant, Z. Tun, R.R. Vold, and R.S. Prosser, "Rarely Observed Phase Transitions in a Novel Lyotropic Liquid Crystal System", *Phys. Rev. Lett.*, **78**:899-902 (1997).
15. M.-P. Nieh, C.J. Glinka, S. Krueger, R.S. Prosser, and J. Katsaras, "SANS Study of the Structural Phases of Magnetically Alignable Lanthanide-Doped Phospholipid Mixtures", *Langmuir*, **17**:2629-2638 (2001).
16. M.-P. Nieh, C.J. Glinka, S. Krueger, R.S. Prosser and J. Katsaras, "SANS Study on the Effect of Lanthanide Ions And Charged Lipids on the Morphology of Phospholipid Mixtures", *Biophys. J.*, **82**:2487-2498 (2002).
17. H. Wang, M.-P. Nieh, E.K. Hobbie, C.J. Glinka, and J. Katsaras, "Kinetic Pathway of the Bilayered-Micelle to Perforated-Lamellae Transition", *Phys. Rev. E*, **67**:060902(1)-060902(4) (2003).
18. M.-P. Nieh, V.A. Raghunathan, H. Wang, and J. Katsaras, "Highly Aligned Lamellar Lipid Domains Induced by Macroscopic Confinement", *Langmuir*, **19**:6936-6941 (2003).
19. M.-P. Nieh, T.A. Harroun, V.A. Raghunathan, C.J. Glinka, and J. Katsaras, "Concentration-Independent Spontaneously Forming Biomimetic Vesicles", *Phys. Rev. Lett.*, **91**:158105(1)-158105(4) (2003).
20. J. Katsaras and K.R. Jeffrey, "Evidence of the Hydration Force in Gel Phase Lipid Multibilayers", *Europhys. Lett.*, **38**:43-48 (1997).
21. J. Katsaras, "Highly Aligned Lipid Membrane Systems in the Physiologically Relevant "Excess Water" Condition", *Biophys. J.*, **73**:2924-2929 (1997).
22. R. Podgornik and V.A. Parsegian, "On a Possible Microscopic Mechanism Underlying the Vapor Pressure Paradox", *Biophys. J.*, **72**:942-952 (1997).
23. J. Katsaras, "Adsorbed to a Rigid Substrate, DMPC Multibilayers Attain Full Hydration in all Mesophases", *Biophys. J.*, **75**:2157-2162 (1998).
24. J.F. Nagle and J. Katsaras, "Absence of a Vestigial Vapor Pressure Paradox", *Phys. Rev. E*, **59**:7018-7024 (1999).
25. R.P. Rand and V.A. Parsegian, "Hydration Forces Between Lipid Bilayers", *Biochim. Biophys. Acta*, **988**:351-376 (1989).
26. J. Katsaras, S. Tristram-Nagle, Y. Liu, R.L. Headrick, E. Fontes, P.C. Mason, and J.F. Nagle, "Clarification of the Ripple Phase of Lecithin Bilayers using Fully Hydrated, Aligned Samples", *Phys. Rev. E*, **61**:5668-5677 (2000).
27. H. Yao, S. Matuoka, B. Tenchov, and I. Hatta, "Metastable Ripple phase of Fully Hydrated Dipalmitoylphosphatidylcholine as Studied by Small Angle X-Ray Scattering", *Biophys. J.*, **59**:252-255 (1991).
28. S. Matuoka, H. Yao, S. Kato, and I. Hatta, "Condition for the Appearance of the Metastable P_β Phase in Fully Hydrated Phosphatidylcholines as Studied by Small-Angle X-Ray Diffraction", *Biophys. J.*, **64**:1456-1460 (1993).
29. M. Rappolt and G. Rapp, "Structure of the Stable and Metastable Ripple-Phase of Dipalmitoylphosphatidylcholine", *Eur. Biophys. J.*, **24**:381-386 (1996).
30. P.C. Mason, B.D. Gaulin, R.M. Epand, G.D. Wignall, and J.S. Lin, "Small-Angle Scattering Studies of the Fully Hydrated Phospholipid DPPC", *Phys. Rev. E*, **59**:921-928 (1999).
31. J. Katsaras and M.J. Watson, "Sample Cell Capable of 100% Relative Humidity Suitable for X-Ray Diffraction of Aligned Lipid Multibilayers", *Rev. Sci. Instrum.*, **71**:1737-1739 (2000).